CHAPTER THIRTEEN

Automated Analysis of Fluorescence Colocalization: Application to Mitophagy

A. Sauvat[*,†,‡,§], H. Zhou[*,†,‡,§,¶], M. Leduc[*,†,‡,§], L.C. Gomes-da-Silva[*,†,‡,§,||], L. Bezu[*,†,‡,§,¶], K. Müller[*,†,‡,§], S. Forveille[*,†,‡,§], P. Liu[*,†,‡,§,¶], L. Zhao[*,†,‡,§,¶], G. Kroemer[*,†,‡,§,¶,||,#,,1], O. Kepp[*,†,‡,§,1]**

[*]Metabolomics and Cell Biology Platforms, Gustave Roussy Comprehensive Cancer Institute, Villejuif, France
[†]Equipe 11 labellisée Ligue contre le Cancer, Centre de Recherche des Cordeliers, Paris, France
[‡]Université Paris Descartes, Sorbonne Paris Cité, Paris, France
[§]Université Pierre et Marie Curie, Paris, France
[¶]University of Paris Sud XI, Kremlin Bicêtre, France
[||]University of Coimbra, Coimbra, Portugal
[#]Pôle de Biologie, Hôpital Européen Georges Pompidou, AP-HP, Paris, France
[**]Karolinska Institute, Karolinska University Hospital, Stockholm, Sweden
[1]Corresponding authors: e-mail address: kroemer@orange.fr; captain.olsen@gmail.com

Contents

Abstract

Mitophagy is a peculiar form of organelle-specific autophagy that targets mitochondria. This process ensures cellular homeostasis, as it fosters the disposal of aged and damaged mitochondria that otherwise would be prone to produce reactive oxygen species and hence endanger genomic stability. Similarly, autophagic clearance of depolarized mitochondria plays a fundamental role in organismal homeostasis as exemplified by the link between Parkinson disease and impaired function of the mitophagy-mediating proteins PINK1 and Parkin. Here, we detail an image-based approach for the quantification of mitochondrial Parkin translocation, which is mechanistically important for the initiation of mitophagy.

Methods in Enzymology, Volume 588
ISSN 0076-6879
http://dx.doi.org/10.1016/bs.mie.2016.09.082

© 2017 Elsevier Inc.
All rights reserved.

1. INTRODUCTION

Autophagy constitutes a phylogenetically conserved adaptive stress response that allows cells to safeguard viability in response to homeostatic perturbations such as malnutrition, shear stress, or chemical cues. This adaptive stress response allows for liberating energy resources on demand and hence safeguards homeostasis via targeted degradation of superfluous, old, or damaged (and hence potentially dangerous) cellular structures (Galluzzi et al., 2015; Galluzzi, Pietrocola, Levine, & Kroemer, 2014; Madeo, Eisenberg, & Kroemer, 2009; Marino, Madeo, & Kroemer, 2011; Sica et al., 2015). The autophagic process involves the formation of double-membraned autophagosomes that engulf cellular material and serve as containment for its lysosomal degradation before metabolic recycling of the autophagic products (Feng, He, Yao, & Klionsky, 2014; Klionsky et al., 2011; Youle & Narendra, 2011).

Mitophagy is a peculiar form of autophagy that culminates in the selective autophagic clearance of damaged mitochondria in response to various mitochondrial stressors leading to the depolarization and/or malfunctioning of the organelle. Similar to macroautophagy, this process involves the sequestration of substrates by double-membraned structures, their closure, and final fusion with lysosomes. The resulting lysosomal acidification and the activation of lysosomal hydrolases drives the cleavage and final recycling of the substrates (Codogno, Mehrpour, & Proikas-Cezanne, 2012; Lamb, Yoshimori, & Tooze, 2013). The recessive Parkinson's disease-linked genes coding for PTEN-induced kinase 1 (PINK1) and PARK2 (better known as Parkin) are functionally important for the clearance of malfunctioning mitochondria. Thus, mutations affecting either PINK1 or Parkin have been found in hereditary forms of Parkinson's disease that are accompanied by the accumulation of dysfunctional mitochondria. PINK1 is continuously imported into healthy mitochondria via the TOMM complex and then degraded. In response to mitochondrial dysfunction and depolarization, PINK1 becomes stabilized and hence more abundant in the outer membrane of mitochondria. PINK1 then recruits the cytoplasmic E3 ubiquitin ligase Parkin to the damaged organelle (Amadoro et al., 2014; Narendra, Tanaka, Suen, & Youle, 2008; Narendra & Youle, 2011) Parkin-dependent ubiquitination of various outer mitochondrial membrane proteins drives the selective targeting of mitochondria by LC3-containining isolation membranes. The engulfment of targeted mitochondria is facilitated by mitochondrial fission

(Buhlman et al., 2014; Twig et al., 2008) that can be reversed by promoting fusion in some models (Deng, Dodson, Huang, & Guo, 2008; Poole et al., 2008). Mitophagosomes fuse with lysosomes to form mitophagolysosomes that specifically localize in perinuclear regions (Eid, Ito, Maemura, & Otsuki, 2013). Lysosomal degradation finally liberates catabolic substrates to counteract cellular stress and reestablish homeostasis.

Here, we detail an exemplary workflow for the microscopic quantitation of mitophagy in Parkin-expressing biosensor cells that mount an adaptive response to mitochondrial depolarization. We applied an R-based algorithm to measure the onset of mitophagy by monitoring the translocation of Parkin to mitochondria. The colocalization of the biosensor with chemically stained mitochondrial structures was accurately quantified based on the global correlation of pixels. This assay may be readily used for the high-throughput assessment of mitophagy in vitro.

2. CELL CULTURE AND TREATMENTS

1. Human osteosarcoma U-2 OS cells stably expressing mCherry-Parkin (Narendra et al., 2008; Zhou et al., 2016), display optimal adherent growth in McCoys medium supplemented with nonessential amino acids, and 10% fetal calf serum (FCS) (see Note 1). Cells are routinely cultured in standard cell culture conditions (37°C, 5% CO_2) in conventional 75 or 175 cm^2 cell culture vessels (see Note 2).
2. Before the monolayer becomes confluent, cells are detached with 0.25% trypsin/EDTA (see Notes 3–9) and seeded in μclear 96-well microplates (Greiner bio-one, Kremsmünster, Austria) (see Notes 10 and 11) in 100 μL of supplemented culture medium. Cells are then allowed to adapt for 24 h.
3. A staining mix is prepared by diluting MitoTracker Green FM (MTG; Molecular Probes, Eugene, OR, USA) in complete medium to a final concentration of 150 n*M*.
4. Cell supernatants are discarded and the cells are incubated with the MitoTracker dye for 20 min at 37°C. Following the cells are rinsed twice with prewarmed complete medium.
5. Cell supernatants are discarded and replaced with 100 μL media supplemented or not with 10 μ*M* or 100 μ*M* carbonyl cyanide m-chlorophenylhydrazone (CCCP; Sigma-Aldrich, St. Louis, MO,

USA) or 5 μ*M* rapamycin (RAPA, R&D Biosystems, Minneapolis, MN, USA).

6. Cells are transferred into an ImageXpress Micro XL automated microscope (Molecular Devices, Sunnyvale, CA, USA) equipped with environmental control (that maintains a humidified atmosphere containing 5% CO_2 at a temperature of 37°C) (see Note 12). All preselected wells are imaged with a 20 min interval for a total of 12 h.

3. ACQUISITION PROCEDURE

1. Perform the imaging using a 20 × objective (see Note 13) and acquire a minimum of four view fields per well (see Note 14).
2. MTG is monitored using a GFP filter set (see Note 15). Adjust the exposure time to achieve an optimal signal-to-noise ratio while avoiding saturated signals.
3. The mCherry-Parkin fusion protein is imaged using a TexasRed filter set (see Note 16). Adjust the acquisition parameters as detailed earlier.
4. Adjust the focal plane for both fluorescences to the same value (see Note 17).
5. The interval for live cell acquisition is set to 20 min (see Note 18) and the acquisition is launched (representative images in Fig. 1A).

4. ASSESSMENT OF COLOCALIZATION: PRINCIPLES

The colocalization of two fluorophores, employed to label different molecules, can be assessed based on two different methods: (i) cooccurrence and (ii) correlation. The first approach consists in quantifying the degree of spatial cooccurrence by enumerating overlapping pixels on the images obtained from one specimen with different optical filters sets, regardless of variations in pixel intensity, whereas the latter assesses the degree of correlation by quantifying the degree of similarity in intensity variations between the fluorescence channels. Results from both methods have to be interpreted with care as cooccurrence is extremely sensitive to image segmentation and can simply reflect close physicochemical properties (e.g., hydrophobic molecules that would attach to membranes), while correlation is very sensitive to background and noise, specifically when the signal-to-noise ratio is low or decreases with time (Adler & Parmryd, 2010).

There are certain limitations to most currently employed methods, i.e., colocalization studies often are performed on a single cell or, in the best case

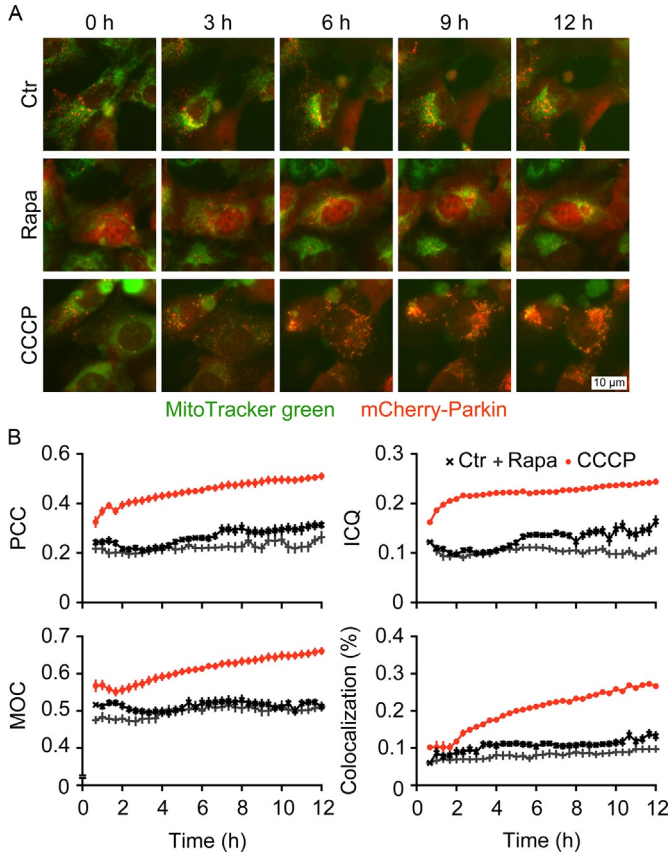

Fig. 1 Quantitative assessment of Parkin translocation in live cell imaging. Mitochondria of human osteosarcoma U-2 OS cells stably expressing Parkin-mCherry were counterstained with MitoTracker green. Thereafter, cells were treated with the mTOR inhibitor rapamycin or the protonophore CCCP at the indicated concentrations. The translocation of Parkin was monitored by live cell microscopy by means of an automated widefield imager at an interval of 20 min for 12 h. Please note that there is an offset in time due to technicalities. Following acquisition, images were analyzed using a custom-built algorithm and different coefficients were calculated. (A) A series of representative images are depicted for each treatment at 0, 3, 6, 9, and 12 h after treatment (size bar equals 10 µm). In panel (B), time-dependent changes in the Pearson correlation coefficient (PCC), Manders overlay coefficient (MOC), intensity correlation quotient (ICQ), and the percent of colocalization in the UNION compartment for mCherry-Parkin and MitoTracker green are reported (mean ± SD, $n = 16$).

scenario, multiple cells in a single image. In both cases, results can hardly be validated independently due to the statistical insignificant number of samples. Furthermore, methods utilized thus far are largely incompatible with the analysis of image-based high-throughput screening- (HTS) and

time-lapse videomicroscopic approaches, due to the extensive number of images generated in both approaches. In addition, the signal-to-noise ratio of many widefield imaging systems is not compatible with most of the colocalization software available today.

In order to adapt colocalization studies to widefield image-based HTS, we decided to develop an algorithm (coded in R) that allows for the efficient assessment of both correlation and cooccurrence in a large set of images acquired on an automated widefield imager. Using the algorithm that was designed for multithreading, thousands of images obtained from videomicroscopic acquisition were analyzed within only few hours (see Note 19).

5. THE R ENVIRONMENT

1. Create the necessary programming environment by installing the free open-source R programming language on your computer (see Notes 20–22).
2. Install the free open-source integrated development interface RStudio (see Notes 23 and 24).
3. Several libraries are necessary to execute the colocalization algorithm. The following libraries can be downloaded and installed within RStudio as packages available from cran.r-project.org : tiff; natural sort; parallel; foreach; doParallel; iterators; reshape. The library EBImage can be downloaded and installed from bioconductor.org by executing the code provided on the website.
4. The source code of the colocalization algorithm is available for download at https://github.com/kroemerlab/HTSColoc. The code has to be executed in the R-environment described earlier, according to the instructions given in the readme.md file retrievable on the website.

6. ASSESSMENT OF COLOCALIZATION: PROTOCOL

1. The database, that contains the image location, together with an unique identifier for the database entry, which in our case was the plate we imaged from on a widefield HTS microscope, are entered as arguments into the algorithm (see Notes 25 and 26). If the analysis computer has no database connection, or the acquired images are not managed by any

database structure, the path to the folder, which contains the images to be analyzed can be furnished instead.

2. Storage location and identifier are loaded into the R environment.
3. For each image a log operator is applied to the original pixel matrix (ORI), and the pixel intensities are then normalized and ranged between 0 and 1 (LOG).
4. Extreme intensity values from ORI are removed so that the distribution of pixel intensities in ORI is adjusted to 0.1–99.9% meaning that only 99.8% of pixels intensities compose the resulting image (NORM).
5. Following a Gaussian filter with a standard deviation of 50 is applied to NORM (GAUSS).
6. GAUSS is subtracted from ORI, while negative pixels are set to 0, and the image is normalized between 0 and 1. (CLEAN).
7. A Top Hat filter, using a structural element defined as a 29-pixels diameter disk, is applied to LOG. Negative pixels are set to 0, and the image is normalized between 0 and 1 (TOP).
8. TOP is binarized using a threshold determined with Otsu's Method. Background pixels are set to 0 and object pixels are set to 1. Single-pixels (connexity 8) are removed from the obtained image (SEG).
9. The Boolean operation OR is applied to SEGs derived from the two channels between which colocalization has to be quantified (UNION).
10. The equivalent operation is realized by using the Boolean operator AND (INTER).
11. Numeric elements from NORM (for the two compared images) are taken where UNION equals 1, and Pearson correlation coefficient (PCC), intensity correlation quotient (ICQ), and Manders overlap coefficient (MOC) are calculated (Fig. 1B).
12. The same operation is realized with INTER, and the overlapping coefficients are calculated (Fig. 1B) (see Notes 27 and 28).

7. CONCLUDING REMARKS

The method presented earlier provides an automated and reliable approach for quantifying mitophagic events by means of monitoring the translocation of Parkin to the mitochondrial membrane in cultured cells responding to chemical or biological cues. The PINK1-dependent aggregation of Parkin at the mitochondrial membrane is one of the initial, functionally important steps of mitophagy. At the next step, the organelle is included by LC3-containining isolation membranes that form a reaction compartment for

the lysosome dependent dissociation of the cargo (Narendra & Youle, 2012). This process is sensitive to the blockage of autophagic degradation by lysosomal fusion inhibitors such as bafilomycin A1 (Yamamoto et al., 1998). Thus in order to underpin the importance of mitophagy and to validate potential hit compounds from HTS campaigns, the decrease in mitochondrial mass that mandatorily follows an increase in mitophagy should be assessed (Narendra et al., 2008). The decrease in mitochondrial mass reflects a direct consequence of lysosomal activity and can therefore be interfered with by lysosomal fusion inhibitors like bafilomycin A1 (Klionsky et al., 2016). The sum of this additional validation steps hence allows for the final interpretations of results obtained from primary screening campaigns. Irrespective of this second line experiments, the described method is suitable to identify chemicals or biologicals with mitophagy-modulatory potential within large libraries and/or with a high temporal resolution.

8. NOTES

1. Optimal cell culture conditions (i.e., culture medium, supplements, and detachment method) for other cell lines might differ from the ones described here. Please refer to your provider.
2. According to the number of experimental conditions and adapting to the given space for maintaining cells, the dimensions of the vessels for cell culture can differ from the ones described here. The ATCC (American tissue type culture collection) recommends T-75 flasks yet to our experience others vessel work equally well.
3. The highest efficacy of trypsin is achieved by minimizing serum content. Rinsing the cells with either PBS or trypsin solution ameliorates detachment in response to trypsin/EDTA.
4. The enzymatic reaction of trypsin works optimal at 37°C and should yield results within 1–3 min. It should be taken care to avoid extended exposure to trypsin in order to minimize cellular stress as it might affect several membrane-related processes.
5. Detachment should be visualized via light microscopy and might vary considerably with cell type and confluency.
6. According to the recommendations of the ATCC U-2 OS cells should be passaged at a ratio of 1:3 to 1:6 with a medium renewal 2–3 times per week to achieve optimal growth (see Note 7).

7. Cells should be kept under exponential growth conditions throughout their culture. Underconfluence should be avoided to circumvent clonal outgrowth (see Note 8). Similarly, overconfluence could lead to oxidative or metabolic stress and has to be avoided.
8. The passage number from an initial stock should not exceed a relatively low, predefined number of passages. New subcultures should be launched from another aliquot of the initial stock to avoid genetic drifts in the cellular population.
9. Maintenance cultures of U-2 OS cell stably expressing mCherry-Parkin were kept under minimal selection pressure by means of geneticin in order to maintain homogenous expression in the cellular population.
10. Five thousand U-2 OS cell stably expressing Parkin fused to mCherry were seeded in μclear 96-well microplates (Greiner bio-one, Kremsmünster, Austria). Geneticin was withdrawn from the culture media to avoid overlapping cellular effects evoked by selection and experiment-specific treatments.
11. The cell culture support might differ from the μclear microplates employed here. The utilized μclear plates are flatbottom plates with physical surface treatment, lid with condensation rings. They are sterile and display a plate bottom thickness of 190 μm (with a batch dependent variation of maximal 10 μm) and plate bottom flatness variation max. 0.6 μm. Using plates with higher plate bottom thickness will necessarily require changing toward a long working distance objective and would therefore influence the properties of the acquired image.
12. The environmental control should be launched well ahead of the start of the experiment to allow the machine to adapt to 37°C. A change in temperature during the imaging process might cause a drift in the *z*-dimension and has to be avoided.
13. The objective employed in our study was a CFI PlanApo Lambda objective (Nikon, Tokio, Japan) with a numerical aperture of 0.75.
14. The number of view fields should be adapted to the confluence of cells at the time of imaging. Thus, a number of view fields that allows for a statistical evaluation should be chosen.
15. In our case the GFP filter set that was used for the acquisition was the GFP-3035D-NTE-ZERO filter set (Semrock, Rochester, NY, USA; 472/30 nm BrightLine single-band bandpass excitation filter/ 520/35 nm BrightLine single-band bandpass emission filter and a 495 nm edge BrightLine single-edge dichroic beamsplitter).

16. Here, we used the TxRed-4040C-NTE-ZERO filter set (Semrock, Rochester, NY, USA; 562/40–25 nm BrightLine single-band bandpass excitation filter/624/40–25 nm BrightLine single-band bandpass emission filter and a 593 nm edge BrightLine single-edge dichroic beam splitter).
17. In the present set up the focus was automatically determined for each acquisition using a laser autofocus that determines the bottom of the well based on the diffraction that causes reflections when the beam passes from gaseous to solid and solid to liquid phase. An additional *z*-offset in order to identify the focal plane with the highest signal-to-noise ratio was defined based on visual inspection and remains unalter during the timeframe of the experiment.
18. The interval for image acquisition has to be chosen based on several considerations: temporal resolution of the observed phenotype, phototoxicity, and fluorochrome exhaustion. Pilot experiments on a limited number of control conditions should yield reproducible results before considering full-blown live cell screening.
19. The software is using multithreading meaning that the number of cores available to the computing unit determines the speed of analysis. In our case a computer equipped with two Intel Xeon E5-2630v2 processors (Santa Clara, CA, USA) each having 6 cores (24 threads) and accessing to 32 GB of RAM was routinely used for the study and allowed to conduct the colocalization analysis within few hours.
20. The R source code can be downloaded at https://www.r-project.org.
21. In our case we used R version 3.3.1 for Windows (Microsoft, Redmond, WA, USA)
22. R precompiled binary versions are provided for various operating systems.
23. Depending on the platform other IDEs are available.
24. In our case we used the RStudio version 0.98.90 for Windows
25. Most modern image-based HTS systems like the one from Molecular Devices employed for this study are furnished together with a dedicated database and database management system. The database requests are designed to work with a SQL database (Microsoft, Redmond, CA, USA) but might be adapted by an experienced user to a given database structure.
26. The algorithm is optimized and has extensively been tested using a 20 × PlanApo objective.

27. Optimal assessment of colocalization depends on several properties of the raw images. Results thus have to be validated by visual inspection prior to HTS approaches.
28. Please consult the documentation available at the download platform for details on the utilized algorithm.

ACKNOWLEDGMENTS

The plasmid coding for mCherry-Parkin was a gift from Richard Youle (Addgene plasmid # 23956). H.Z. and P.L. are supported by the China Scholarship Council, L.Z. is supported by the Ligue contre le Cancer, G.K. is supported by the Ligue contre le Cancer (équipes labelisées); Agence National de la Recherche (ANR)—Projets blancs; ANR under the frame of E-Rare-2, the ERA-Net for Research on Rare Diseases; Association pour la recherche sur le cancer (ARC); Cancéropôle Ile-de-France; Institut National du Cancer (INCa); Fondation Bettencourt-Schueller; Fondation de France; Fondation pour la Recherche Médicale (FRM); the European Commission (ArtForce); the European Research Council (ERC); the LabEx Immuno-Oncology; the SIRIC Stratified Oncology Cell DNA Repair and Tumor Immune Elimination (SOCRATE); the SIRIC Cancer Research and Personalized Medicine (CARPEM); the Swiss Bridge Foundation, ISREC and the Paris Alliance of Cancer Research Institutes (PACRI).

Legal disclaimer: The described algorithm is for noncommercial purposes only. The authors are not responsible for any consequences resulting from the use of the algorithm or the R environment.

REFERENCES

Adler, J., & Parmryd, I. (2010). Quantifying colocalization by correlation: The Pearson correlation coefficient is superior to the Mander's overlap coefficient. *Cytometry Part A*, *77*(8), 733–742. http://dx.doi.org/10.1002/cyto.a.20896.

Amadoro, G., Corsetti, V., Florenzano, F., Atlante, A., Ciotti, M. T., Mongiardi, M. P., … Calissano, P. (2014). AD-linked, toxic NH2 human tau affects the quality control of mitochondria in neurons. *Neurobiology of Disease*, *62*, 489–507. http://dx.doi.org/10.1016/j.nbd.2013.10.018.

Buhlman, L., Damiano, M., Bertolin, G., Ferrando-Miguel, R., Lombes, A., Brice, A., & Corti, O. (2014). Functional interplay between Parkin and Drp1 in mitochondrial fission and clearance. *Biochimica et Biophysica Acta*, *1843*(9), 2012–2026. http://dx.doi.org/10.1016/j.bbamcr.2014.05.012.

Codogno, P., Mehrpour, M., & Proikas-Cezanne, T. (2012). Canonical and non-canonical autophagy: Variations on a common theme of self-eating? *Nature Reviews Molecular Cell Biology*, *13*(1), 7–12. http://dx.doi.org/10.1038/nrm3249.

Deng, H., Dodson, M. W., Huang, H., & Guo, M. (2008). The Parkinson's disease genes pink1 and parkin promote mitochondrial fission and/or inhibit fusion in Drosophila. *Proceedings of the National Academy of Sciences of the United States of America*, *105*(38), 14503–14508. http://dx.doi.org/10.1073/pnas.0803998105.

Eid, N., Ito, Y., Maemura, K., & Otsuki, Y. (2013). Elevated autophagic sequestration of mitochondria and lipid droplets in steatotic hepatocytes of chronic ethanol-treated rats: An immunohistochemical and electron microscopic study. *Journal of Molecular Histology*, *44*(3), 311–326. http://dx.doi.org/10.1007/s10735-013-9483-x.

Feng, Y., He, D., Yao, Z., & Klionsky, D. J. (2014). The machinery of macroautophagy. *Cell Research*, *24*(1), 24–41. http://dx.doi.org/10.1038/cr.2013.168.

Galluzzi, L., Pietrocola, F., Bravo-San Pedro, J. M., Amaravadi, R. K., Baehrecke, E. H., Cecconi, F., … Kroemer, G. (2015). Autophagy in malignant transformation and cancer progression. *The EMBO Journal*, *34*((7), 856–880. http://dx.doi.org/10.15252/embj.201490784.

Galluzzi, L., Pietrocola, F., Levine, B., & Kroemer, G. (2014). Metabolic control of autophagy. *Cell*, *159*(6), 1263–1276. http://dx.doi.org/10.1016/j.cell.2014.11.006.

Klionsky, D. J., Abdelmohsen, K., Abe, A., Abedin, M. J., Abeliovich, H., Acevedo Arozena, A., … Zughaier, S. M. (2016). Guidelines for the use and interpretation of assays for monitoring autophagy (3rd edition). *Autophagy*, *12*(1), 1–222. http://dx.doi.org/10.1080/15548627.2015.1100356.

Klionsky, D. J., Baehrecke, E. H., Brumell, J. H., Chu, C. T., Codogno, P., Cuervo, A. M., … Tooze, S. A. (2011). A comprehensive glossary of autophagy-related molecules and processes (2nd edition). *Autophagy*, *7*(11), 1273–1294. http://dx.doi.org/10.4161/auto.7.11.17661.

Lamb, C. A., Yoshimori, T., & Tooze, S. A. (2013). The autophagosome: Origins unknown, biogenesis complex. *Nature Reviews. Molecular Cell Biology*, *14*(12), 759–774. http://dx.doi.org/10.1038/nrm3696.

Madeo, F., Eisenberg, T., & Kroemer, G. (2009). Autophagy for the avoidance of neurodegeneration. *Genes & Development*, *23*(19), 2253–2259. http://dx.doi.org/10.1101/gad.1858009.

Marino, G., Madeo, F., & Kroemer, G. (2011). Autophagy for tissue homeostasis and neuroprotection. *Current Opinion in Cell Biology*, *23*(2), 198–206. http://dx.doi.org/10.1016/j.ceb.2010.10.001.

Narendra, D., Tanaka, A., Suen, D. F., & Youle, R. J. (2008). Parkin is recruited selectively to impaired mitochondria and promotes their autophagy. *The Journal of Cell Biology*, *183*(5), 795–803. http://dx.doi.org/10.1083/jcb.200809125.

Narendra, D. P., & Youle, R. J. (2011). Targeting mitochondrial dysfunction: Role for PINK1 and Parkin in mitochondrial quality control. *Antioxidants & Redox Signaling*, *14*(10), 1929–1938. http://dx.doi.org/10.1089/ars.2010.3799.

Narendra, D. P., & Youle, R. J. (2012). Neurodegeneration: Trouble in the cell's powerhouse. *Nature*, *483*(7390), 418–419. http://dx.doi.org/10.1038/nature10952.

Poole, A. C., Thomas, R. E., Andrews, L. A., McBride, H. M., Whitworth, A. J., & Pallanck, L. J. (2008). The PINK1/Parkin pathway regulates mitochondrial morphology. *Proceedings of the National Academy of Sciences of the United States of America*, *105*(5), 1638–1643. http://dx.doi.org/10.1073/pnas.0709336105.

Sica, V., Galluzzi, L., Bravo-San Pedro, J. M., Izzo, V., Maiuri, M. C., & Kroemer, G. (2015). Organelle-specific initiation of autophagy. *Molecular Cell*, *59*(4), 522–539. http://dx.doi.org/10.1016/j.molcel.2015.07.021.

Twig, G., Elorza, A., Molina, A. J., Mohamed, H., Wikstrom, J. D., Walzer, G., … Shirihai, O. S. (2008). Fission and selective fusion govern mitochondrial segregation and elimination by autophagy. *The EMBO Journal*, *27*(2), 433–446. http://dx.doi.org/10.1038/sj.emboj.7601963.

Yamamoto, A., Tagawa, Y., Yoshimori, T., Moriyama, Y., Masaki, R., & Tashiro, Y. (1998). Bafilomycin A1 prevents maturation of autophagic vacuoles by inhibiting fusion between autophagosomes and lysosomes in rat hepatoma cell line, H-4-II-E cells. *Cell Structure and Function*, *23*(1), 33–42.

Youle, R. J., & Narendra, D. P. (2011). Mechanisms of mitophagy. *Nature Reviews. Molecular Cell Biology*, *12*(1), 9–14. http://dx.doi.org/10.1038/nrm3028.

Zhou, H., Forveille, S., Sauvat, A., Yamazaki, T., Senovilla, L., Ma, Y., … Kroemer, G. (2016). The oncolytic peptide LTX-315 triggers immunogenic cell death. *Cell Death & Disease*. 7, e2134. http://dx.doi.org/10.1038/cddis.2016.47.